Journal of Materials Chemistry A

Accepted Manuscript

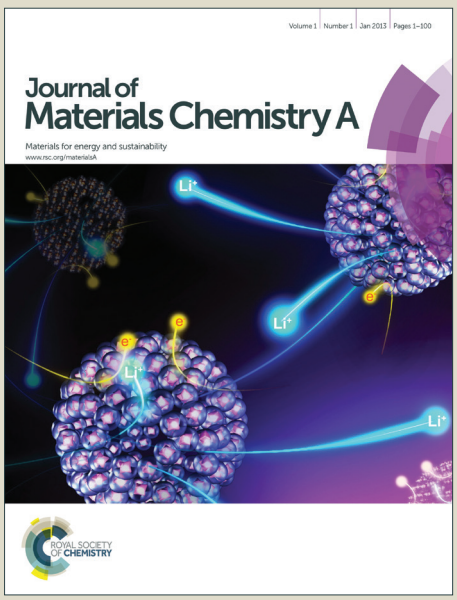

ROYAL SOCIETY OF CHEMISTRY

www.rsc.org/materialsA

Journal of

Materials Chemistry A

RSCPublishing

Paper

TiO_2-supported copper nanoparticles prepared via ion exchange for photocatalytic hydrogen production

Cite this: DOI: 10.1039/x0xx00000x

Received ooth January 2012,
Accepted ooth January 2012

DOI: 10.1039/x0xx00000x

www.rsc.org/MaterialsA

Hao Tian, Xiaoli Zhang*, Jason Scott, Charlene Ng and Rose Amal*

Abstract: Ion exchange (IE) has been used to prepare Cu/TiO_2 for photocatalytic hydrogen generation. The IE Cu/TiO_2 particles comprised a mixture of large and fine copper/copper oxide deposits which were well dispersed across the TiO_2 surface. Hydrogen generation photoactivity by the IE Cu/TiO_2 was ~44 % greater than the activity displayed by Cu/TiO_2 prepared via wet impregnation (WI) at a similar copper loading. Temperature programmed reduction studies indicated the IE Cu/TiO_2 possessed a greater portion of highly dispersed fine copper deposits than the WI Cu/TiO_2 which may account for the higher photoactivity. The hydrogen generation activity of IE Cu/TiO_2 was maintained over three 5 h reaction cycles.

1. Introduction

Being the most abundant element on earth, hydrogen is considered as a very promising alternative energy carrier to reduce the energy dependence on the future depletion of fossil fuels.[1] Most of the present hydrogen sources are derived from fossil fuels by methane steam reforming.[2] Alternately, the utilization of photocatalysts for energy conversion to produce hydrogen from biomass derivatives such as methanol is considered to be an attractive and sustainable approach.

TiO_2 has been widely utilized as a photocatalyst owing to its exceptional properties such as suitable band edges for redox reactions, biological and chemical inertness, availability, environmental friendliness, low cost, and long-term stability against photo- and chemical-corrosion.[3-6] However, due to fast recombination of the excited electron/hole pairs and the conduction band potential of TiO_2 not being sufficiently negative for the redox potential of H^+/H_2, hydrogen generation efficiency over bare TiO_2 is low.[3] For effective hydrogen production, TiO_2 needs to be modified with a noble metal such as Pt,[7] Au[8] or Pd,[9] which have proved to be very effective. However, these noble metals are expensive and rare. Thus, alterative metals that are cheap, abundant and capable of promoting photocatalytic activity have garnered considerable attention.

Copper is one such metal and is of growing interest for large scale solar energy conversion technologies.[10] Cu-containing TiO_2 has proven to be capable of enhancing the hydrogen production efficiency of TiO_2.[11-17] Much of the research has utilized wet impregnation (WI) to load the copper onto the TiO_2 in the form of CuO and/or Cu_2O. Limited research has been reported on the synthesis and activity of metallic copper loaded TiO_2 for photocatalytic hydrogen production.

During conventional WI, active metal species agglomerate inhomogeneously at the grain boundary of the support especially at a higher copper concentration, leading to the formation of large nanoparticles.[18] Sodesawa et al. and Liu et al. found increased deactivation of their Cu/SiO_2 catalyst during methanol dehydrogenation which arose from a lower copper surface area invoked by the WI synthesis method.[19, 20] Sodesawa et al. also reported catalyst deactivation was less significant for Cu/SiO_2 prepared via an ion exchange (IE) process due to a better dispersion of copper on the silica support.[19] Hence, the IE method represents a technique that can overcome agglomeration and deactivation arising from the facile reaction conditions during the chemical conversion process. The IE method has been highlighted as a strategy with a simple and rapid chemical reaction step at room temperature. It can promote the formation of new phases and compositions which is often kinetically controllable rather than thermodynamically dependent.[21] The IE method is a facile and energy-lean technique, useful for synthesizing new nanomaterials with improved activities at a low-cost.

Herein, the IE method has been used as the foundation for preparing a TiO_2 photocatalyst loaded with copper nanoparticles. The IE Cu/TiO_2 has been assessed as a photocatalyst for hydrogen generation and its performance compared with Cu/TiO_2 prepared using WI. Characterization of the materials was used to identify properties of the IE Cu/TiO_2

as well as understand activity differences between it and the WI Cu/TiO_2.

2. Experimental

2.1 Reagents

Aeroxide P25 titanium dioxide (80% anatase, 20% rutile (Sigma-Aldrich)), sodium hydroxide (Ajax Finechem), hydrochloric acid (32 vol%, Ajax Finechem), copper nitrate (Ajax Finechem), copper sulphate (Ajax Finechem) and methanol (Sigma-Aldrich) were used without further purification.

2.2 Material synthesis

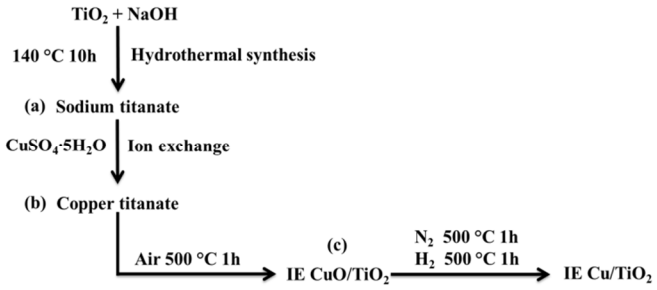

Scheme 1. Synthesis procedure for IE Cu/TiO_2.

The preparation of IE Cu/TiO_2 involves four key stages (Scheme 1), namely: (1) the hydrothermal synthesis of sodium titanate; (2) ion-exchange between copper and sodium to produce copper titanate; (3) the copper titanate in air to produce IE CuO/TiO_2; (4) reducing the IE CuO/TiO_2 to give IE Cu/TiO_2.

a) Sodium titanate synthesis

Aeroxide P25 (2 g) was suspended in 100 ml deionized water with 48 g of NaOH (Ajax Finechem) added into the suspension. Following stirring for 30 mins, the suspension was hydrothermally treated at 140 °C for 10 hour. After the reaction was completed, the precipitate was recovered and washed with water until pH 12 was attained whereby it was rinsed with ethanol to remove the residual surface OH^- and Na^+. The samples were dried at 60 °C overnight.[22-24]

b) Copper titanate synthesis

The sodium titanate (0.3 g) was allowed to react with 30 mL of 0.07 mol/L $CuSO_4$ solution ($CuSO_4{\cdot}5H_2O$) for 24 hours at room temperature. To achieve Cu^{2+} saturation, a second ion-exchange process was performed. The exchanged titanates were separated and washed once with water and twice with ethanol to avoid physical adsorption of the substituting ions on the surface. The samples were dried at 60 °C overnight.

c) IE CuO/TiO_2 and IE Cu/TiO_2 synthesis

Copper titanate obtained from the IE process was calcined in air (25 ml/min) at a rate of 1.7 °C /min to 500 °C for 1 hour to obtain IE CuO/TiO_2.To prepare IE Cu/TiO_2 the IE CuO/TiO_2 was reductively annealed in N_2 (25 ml/min) at 500°C for 1 hour followed by pure H_2 (30 ml/min) at 500 °C for 1 hour. ICP analysis indicated a 0.2 wt% residual Na^+ loading of was present in the annealed sample.

d) WI CuO/TiO_2 and WI Cu/TiO_2 synthesis

WI CuO/TiO_2 and WI Cu/TiO_2 were prepared by impregnating 2 g of Aeroxide P25 with a 150 mL solution of 0.05 mol/L $Cu(NO_3)_2$ followed by drying at 110 °C for 10h. WI CuO/TiO_2 and Cu/TiO_2 were obtained following the same calcination process as described above for the IE samples.

e) Neat IE TiO_2 synthesis

The sodium titanate was washed with 0.1M HCl and then with ultra-pure water until the pH of the supernatant (following centrifuging) reached approximately 5. The washed particles were then dried at 70 °C overnight after which they were calcined under the same conditions used to produce IE Cu/TiO_2.

2.3 Characterization

Crystal and structural characteristics of the products were investigated by powder X-ray diffraction (XRD) performed on a Philips X'pert multipurpose X-ray diffraction system with monochromatized Cu Kα radiation (λ =1.5418 Å). Sample morphology was assessed by transmission electron microscopy equipped with an energy dispersion X-ray spectrometer (TEM, JEOL 1400 and Phillips CM200 including HRTEM). Optical properties of the samples were characterized by UV-visible spectroscopy (Shimadzu UV-3600). $BaSO_4$ was used as a reflectance standard in a UV-vis diffuse reflectance experiment. The surface chemical composition was characterized using an X-ray photoemission spectrometer (XPS, ESCALAB220i-XL, Thermo Scientific) with Al Kα at 1486.6 eV. All the XPS data were calibrated by the carbon 1s peak at 285 eV. The surface area and pore size distribution were determined by N_2 adsorption (BET method, Micromeritics Tristar). Copper loading of IE Cu/TiO_2 and WI Cu/TiO_2 were determined by Inductively Coupled Plasma Mass Spectroscopy ICPMS integrated with an ESI-NewWave NWR213 Laser Ablation accessory.

Hydrogen temperature-programmed reduction (H_2-TPR) was conducted on a Micromeritics Autochem II 2920. To be able to identify reducibility of the copper species on the surface IE CuO/TiO_2 and WI CuO/TiO_2 were used instead of IE Cu/TiO_2 and WI Cu/TiO_2. In a typical experiment, approximately 50 mg of catalyst sample was pretreated in Ar (20 ml/min) at 150 °C for 0.5 h and then cooled to 50 °C. The sample was then heated at a rate of 10 °C /min to 500 °C in a reducing gas flow of 5% H_2-Ar (40 ml/min) and hydrogen consumption was monitored.

Copper dispersion was determined by dissociative N_2O adsorption using the procedure described by Van Der Grift et al.[25] The sample was initially reduced by the same procedure described for H_2-TPR. After it cooled to 50 °C, passivation was performed by exposing the reduced catalyst to a flow of 20% N_2O in N_2 (20 ml/min) mixed with Ar (20 ml/min) for 30 min. After passivation, the catalyst was purged with Ar (20 ml/min) for 60 min to remove residual N_2O and subjected to another H_2-TPR cycle as described above.

2.4 Photocatalytic hydrogen production

Photocatalytic activity was assessed by studying the hydrogen generation from a 10% methanol by volume (90% ultra-pure water) solution. A single-neck reaction flask was loaded with 25 mL of the methanol solution containing 25 mg of photocatalyst. The reaction mixture was purged with Ar gas for 30 min to remove oxygen after which it was illuminated with a 300 W Xe lamp for 5 h. A water jacket was used to cool the system. Gas samples (1.0 ml) were taken at 30 min intervals

and injected into a Shimadzu GC-8A gas chromatograph containing a Hayesep DB 100/120 column. Over the 5 hour experiment time frame the solution temperature was observed to increase to 45 °C. To identify the contributions of the neat IE TiO_2 and Aeroxide P25 supports to photocatalytic activity control experiments using these materials were performed.

3. Results and discussion

Figure 1(a) contains the XRD patterns of the hydrothermally synthesized sodium titanate and ion-exchanged copper titanate. The bottom profile exhibits the main peaks of sodium titanate which can be indexed to $Na_2Ti_3O_7{\cdot}nH_2O$ (JCPDS no. 72-0148)[22, 23] and indicates an interlayer spacing (d_{100}) of 0.925nm. The TiO_6 octahedra link to form layers possessing negative electrical charges while the sodium cations exist between these octahedral layers. The layered sodium titanate structure yields a high specific surface area (343 m^2/g), which is advantageous for the ion-exchange process.[24] After the Cu^{2+} ion exchange process the interlayer distance of the titanate decreases to 0.857 nm suggesting a greater interaction between the copper ions and the negatively charged layers. Furthermore, it is apparent that most of the titanate peaks shift to a higher angle after the ion-exchange process, especially the (020) peak. This indicates the crystalline unit cell reduced and can be attributed to the replacement of Na^+ with Cu^{2+}.

Figure 1(b) provides the Raman spectra of the sodium titanate and IE copper titanate. The peak near 908 cm^{-1} in sodium titanate is attributed to the short Ti–O stretching vibration involving non-bridging oxygen atoms that are coordinated with Na^+. After the ion-exchange process, the new peak at lower frequencies (825 cm^{-1}) is assigned to the short Ti-O vibration affected by Cu^{2+}.[23] Similar XRD and Raman results are consistent with the findings reported by Zhang and colleagues.[23] Additionally, oxygen, copper and titanium elements are all homogeneously distributed across the IE

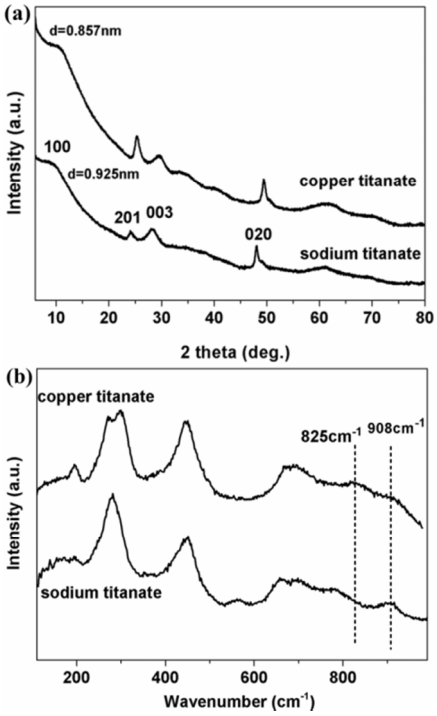

Figure 1. (a) XRD patterns; (b) Raman profiles of hydrothermally synthesised sodium titanate and ion exchanged copper titanate.

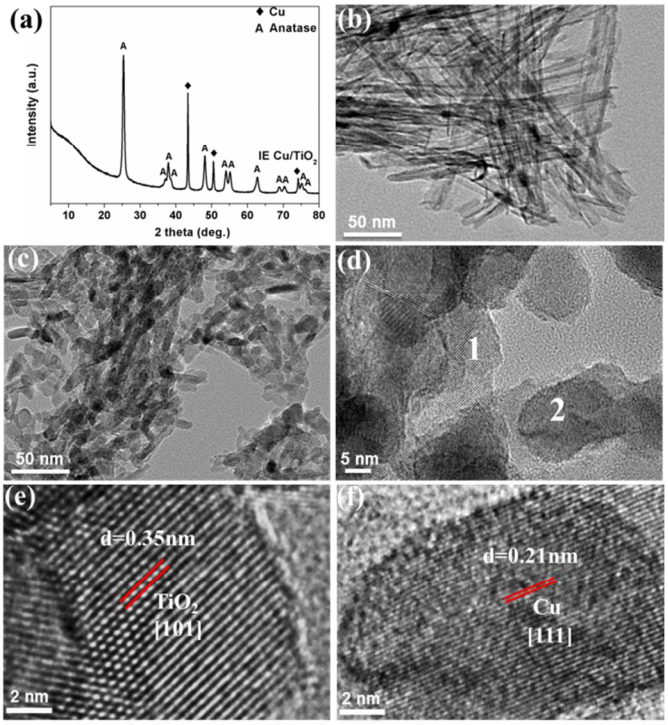

Figure 2. (a) XRD pattern of IE Cu/TiO_2; (b) TEM image of ion-exchanged copper titanate; (c) TEM images of IE Cu/TiO_2; (d),(e),(f) HRTEM images of IE Cu/TiO_2. Images of (e) and (f) are enlarged images at location 1 and 2 in image (d).

copper titanate as confirmed by elemental mapping (Supplementary information, Figure S1), providing strong support for a successful ion-exchange process.

The XRD pattern of IE Cu/TiO_2 is shown in Figure 2(a). Anatase is the only phase of TiO_2 (JCPDS no. 71-1166) present in the IE Cu/TiO_2. The diffraction peaks of IE Cu/TiO_2 at 2θ=43.5°, 50.5° and 74.3° can be attributed to the metallic Cu (JCPDS no. 70- 3039) crystalline structure with plane orientations of (111), (200) and (220), respectively. Based on the (111) Cu peak, the Scherrer equation estimated the Cu^0 crystallite size to be 36.4 nm (Table 1). Following calcination, the powder was purple in colour also suggesting the presence of small metallic copper particles on the TiO_2 surface. From ICP-MS the Cu loading (mass %) was determined to be approximately 19% (Table 1). In addition, 0.2 wt% of elemental sodium was detected in the sample, indicating almost complete exchange of the Na^+ by Cu^{2+} has occurred.

HRTEM analysis (Supplementary information, Figure S2) confirms the sodium titanate possesses a nanosheet structure. Similar morphologies were reported by Zhang et al. [23] and Li et al. [24] The Cu^{2+} ion exchange process did not appear to alter the titanate structure as illustrated in Figure 1b. As depicted in Figure 1c, calcining at 500 °C leads to complete structural collapse of the layered structure. This results in a mixture of elongated and irregularly shaped particles. Elemental mapping (Supplementary information, Figure S3) shows the calcination process has minimal impact on element distribution with the copper, oxygen and titanium remaining homogeneously distributed within the IE Cu/TiO_2. HRTEM images of the IE Cu/TiO_2 (Figures 1d, e and f) show two types of lattice fringes are present with spacings of 0.35 nm and 0.21 nm. These d-spacings are in good agreement with the spacing of the (101)

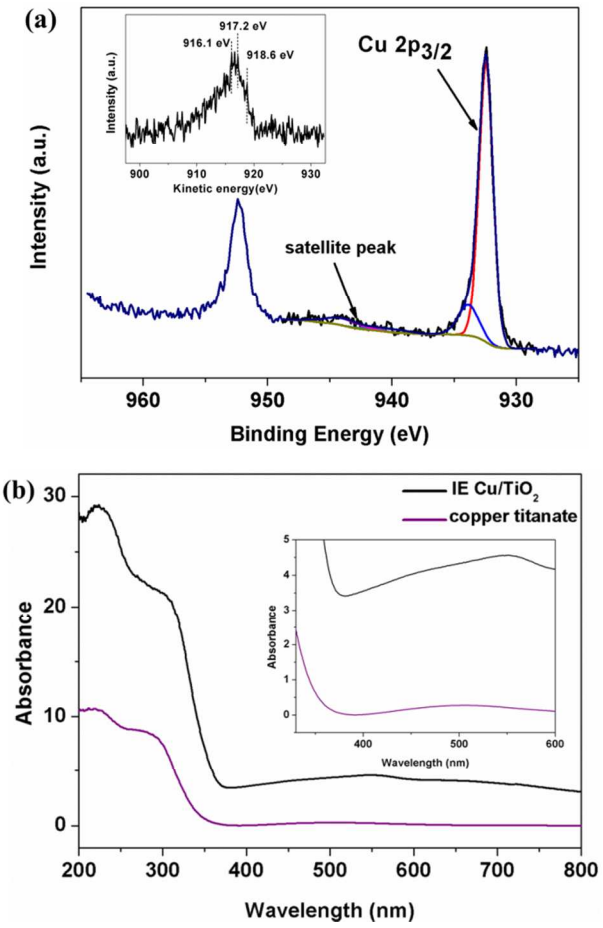

Figure 3. (a) XPS spectra depicting Cu 2p3/2 core levels from IE Cu/TiO_2. Insert is Cu LMM Auger spectrum of IE Cu/TiO_2. (b) UV/Vis absorption spectra of ion-exchanged copper titanate and IE Cu/TiO_2. Insert is the adsorption spectra from 340 nm to 600 nm.

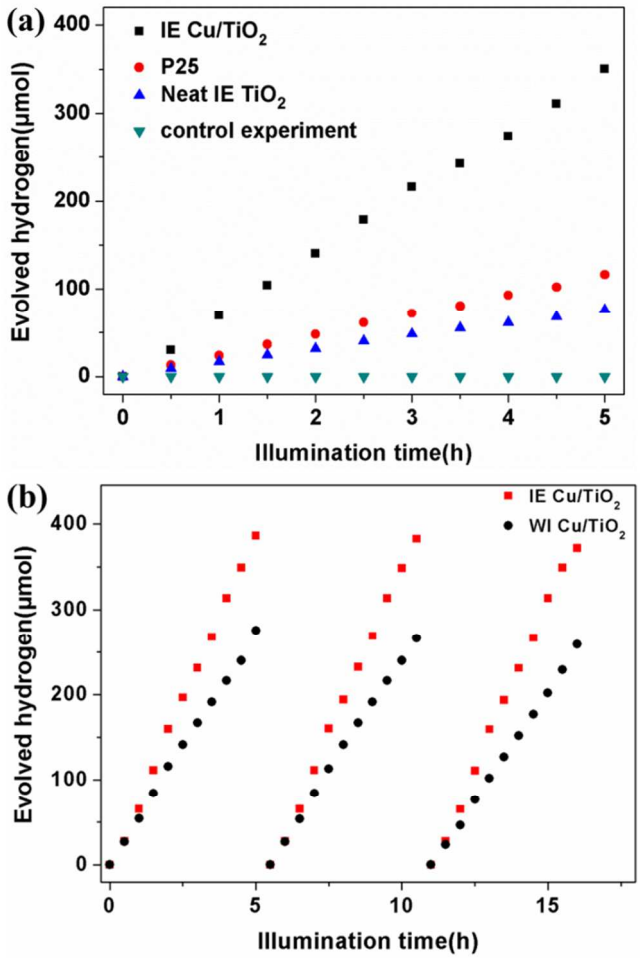

Figure 4. (a) Comparison of photocatalytic H_2 generated from a 10 % methanol solution for IE Cu/TiO_2, neat Aeroxide P25, neat IE TiO_2 and a control experiment (no irradiation or photocatalysts); (b) Photocatalytic activity of IE Cu/TiO_2 and WI Cu/TiO_2 during repeated hydrogen generation cycles.

plane of anatase TiO_2 and the (111) planes of Cu metal, respectively, verifying the presence of TiO_2 and metallic copper in the calcined material.

XPS analysis of IE Cu/TiO_2 (Figure 3a) indicates a dominant Cu 2p3/2 core peak situated at 932.5 eV corresponding to the presence of Cu^+ and/or Cu^0. The smaller peak at 934.2 eV in conjunction with the shakeup satellite peak (at 944.1 eV) is assigned to Cu 2p3/2 in CuO. As the binding energy values of Cu^+ and Cu^0 are located at a similar position, distinction between these two oxidation states is only feasible upon examination of the Cu LMM Auger spectra (Figure 3a inset).[26, 27] The peak at 918.6 eV of the Cu LMM Auger kinetic energy curve for IE Cu/TiO_2 indicates the presence of metallic copper. The two peaks centered at 916.1 eV and 917.2 eV approach the values of bulk Cu_2O and CuO, respectively.[28] The presence of Cu^+ and Cu^{2+} may derive from the surface of the Cu^0 deposits undergoing oxidation upon exposing the sample to air.[29] Furthermore, Cu_2O and CuO were not observed in the IE Cu/TiO_2 XRD spectra as shown earlier in Figure 2a. The inability of XRD to detect Cu_2O or CuO is likely to derive from the resolution of the technique providing information mainly on the bulk particle and not the surface. Coupling the XRD, TEM and XPS findings together, it appears the copper exists on the TiO_2 surface as copper metal crystallites with an oxidised shell and/or smaller (or amorphous) Cu-oxide deposits.

The absorption spectra for ion-exchanged copper titanate and IE Cu/TiO_2 are shown in Figure 3b. The ion-exchanged copper titanate displays absorption across the visible light region ascribed to the d-d transition of copper metal ions as reported by Li and his colleagues.[24] The IE Cu/TiO_2 also exhibits absorption in the visible light absorption band which could be due to absorption by the metallic Cu (225-590 nm).[30]

Photocatalytic hydrogen production activities in a 10 vol% methanol solution are provided in Figure 4. Included in the figure are activities for IE Cu/TiO_2, neat IE TiO_2, neat Aeroxide P25, and a control experiment (no irradiation or photocatalyst present). The control experiment shows no hydrogen is generated in the absence of irradiation and a photocatalyst, confirming hydrogen is generated by the photocatalytic process. The neat IE TiO_2 and neat Aeroxide P25 are photoactive towards hydrogen generation (76 μmol and 116 μmol, respectively, over 5 h) as illustrated in Figure 4a. XRD analysis of the neat IE TiO_2 (Supplementary information, Figure S4) indicated the TiO_2 was in the form of anatase. Despite the conduction band potential of anatase being more negative than the reduction potential of H^+/H_2, the neat TiO_2 (both IE TiO_2 and P25) is not very efficient at photocatalytically generating hydrogen. Photocatalytic hydrogen generation by the IE Cu/TiO_2 is more than three times greater than the neat material (350 μmol over 5 h) illustrating the activity enhancement

invoked by the Cu presence. Song et al. described the mechanism for photocatalytic reaction using copper metal loaded TiO_2.[31] They stated the photogenerated electrons migrated to the surface of photocatalyst and were injected into the copper metal. Meanwhile, the photogenerated holes remained within the host photocatalyst. Metallic copper was considered to be the active oxidation state for hydrogen generation. The Fermi energy level of metallic copper (work function, Φ, = 4.65 eV) lay below the TiO_2 conduction band whereby photogenerated electrons could be easily transferred to the metallic copper, decreasing electron-hole recombination. Sun et al. described the presence of Cu_2O and metallic copper in their CuO/TiO_2 after photocatalytic hydrogen production indicating excited electrons in the TiO_2 conduction band reduced the CuO deposits.[11] Yu et al. also reported electrons were transferred from the conduction band of TiO_2 to $Cu(OH)_2$ clusters in their $Cu(OH)_2$-modified TiO_2 leading to the reduction of Cu^{2+} to metallic copper.[32] In our work the metallic component of the copper deposits gave the IE Cu/TiO_2 a purple hue. The purple colour was retained during the hydrogen generation reaction implying the copper remained in its metallic state.

As mentioned earlier copper is most commonly loaded onto photocatalytic supports using wet impregnation. In addition, Aeroxide P25 is commonly used as the photocatalytic support. On this basis we prepared WI Cu/TiO_2 with a similar Cu loading to the IE Cu/TiO_2 (Table 1) for comparative purposes. The contrast in photocatalytic hydrogen generation by the two Cu/TiO_2 materials is provided in Figure 4(b). Also included in the figure is the activity for three hydrogen generation cycles. Over the five hour period (first cycle) the IE Cu/TiO_2 produced hydrogen at an average rate of 76 µmol/hr, which was 44% greater than the WI Cu/TiO_2. This equates to apparent quantum efficiencies of 3.44% and 2.40% by the IE Cu/TiO_2 and WI Cu/TiO_2, respectively. Moreover, both IE Cu/TiO_2 and WI Cu/TiO_2 retained their activity levels over the three cycles.

The XRD profile for WI Cu/TiO_2 (Supplementary information, Figure S5a) indicates copper exists on the P25 support in a metallic state, similar to the IE Cu/TiO_2. The copper (111) peak indicates the WI copper crystallites are larger in size than the IE Cu/TiO_2 (Table 1). Additionally, XRD indicates the TiO_2 crystal size of the IE Cu/TiO_2 (18.2 nm) is smaller than the WI Cu/TiO_2 (23.4 nm) which, in conjunction with the different copper crystallite sizes, helps account for the differences in surface area between the two materials. TEM imaging of the WI Cu/TiO_2 (Figure S5b) shows the particles have sizes over the range 21 to 46 nm supporting the values obtained from the XRD profile. The higher overall surface area of the IE Cu/TiO_2 may be a contributing factor to the better activity as it can facilitate greater surface adsorption of the reactants in turn promoting interfacial charge transfer.[33]

Other textural properties of the two materials, including copper metal dispersion, surface area and crystal diameter (from dissociative N_2O adsorption) are summarized in Table 1. Dissociative N_2O adsorption indicates the IE Cu/TiO_2 (30.4%)

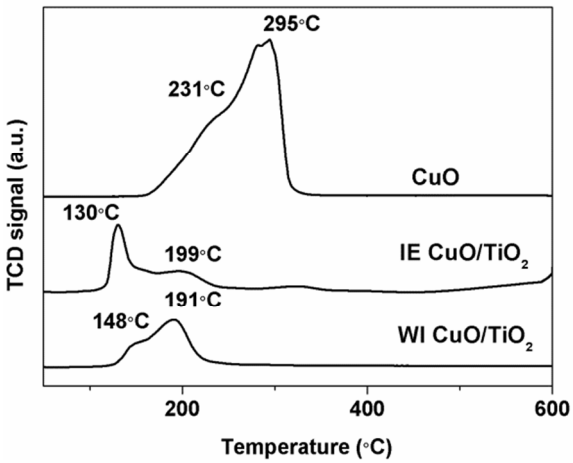

Figure 5. H_2 temperature program reduction profiles of CuO, IE CuO/TiO_2 and WI CuO/TiO_2.

has a ~50% greater copper dispersion than WI CuO/TiO_2 with a similar variance in the surface area of the exposed metal. The difference in copper dispersion between the two materials is also reflected by the XPS results (Figure 3(a) and Figure S6 (Supporting information)). The Cu/Ti ratio (from XPS) is indicative of metal dispersion with a larger ratio signifying greater dispersion.[34, 35] That is, the Cu/Ti ratio for IE Cu/TiO_2 (0.098) is greater than ratio for WI Cu/TiO_2 (0.082) giving qualitative support to the dispersion values from N_2O dissociation.

There is however a considerable discrepancy between the copper deposit diameters estimated from the N_2O dissociation studies and the crystallite sizes calculated by the Scherrer equation from the XRD profiles. The values obtained for N_2O dissociation mirror the higher crystallite size of the WI CuO/TiO_2 but are approximately a factor of 10 times lower than the values from XRD. The apparent discrepancy may arise from the copper being present on the surface as more than one structure with the nature of each analysis technique detecting one structure over another. For example, XRD is more a bulk analysis technique (and is also adept at detecting only crystalline materials) so will favour identifying the characteristics of larger, crystalline deposits at the expense of co-existing smaller ones. N_2O dissociation is a surface analysis technique so will probe all deposits, irrespective of size or crystallinity. Consequently, the XRD and N_2O dissociation findings suggest the copper exists in at least two forms: (1) larger metallic copper deposits from XRD (supported by HRTEM) and (2) fine copper deposits suggested by N_2O dissociation. XPS analysis gave a mixture of copper oxidation states for both samples which could be due to an oxidised surface layer of the larger copper deposits and /or the fine copper deposits existing in an oxidised state.

The H_2-TPR profiles of IE CuO/TiO_2 and WI CuO/TiO_2 in Figure 5 support the notion of at least two types of copper

Table 1 Physical properties of IE Cu/TiO_2 and WI Cu/TiO_2

Samples	Copper loading(%)	Specific Surface Area[a](m^2/g)	Copper average crystalline size[b](nm)	Copper dispersion[c](%)	Copper surface area [c](m^2 Cu/g Cu/TiO_2)	Copper average volume-surface diameter[c](nm)
IE Cu/TiO_2	18.9	74	36.4	30.4	39	3.3
WI Cu/TiO_2`	18.4	27	48.3	20.2	25	5.0

[a]Evaluated from N_2 physisorption using the BET model.
[b]Calculated using the Scherrer equation for the Cu(111) peak in the XRD profiles.
[c]Calculated using dissociative N_2O adsorption.[25]

deposits existing on the TiO_2 support. The IE CuO/TiO_2 profile possesses two distinct reduction peaks: (1) a high intensity peak centered at 130 °C and (2) a broader peak centered at 198 °C. The WI CuO/TiO_2 profile also exhibits two distinct peaks: (1) a lower intensity peak at 148 °C which shoulders a (2) higher intensity peak at 191 °C. All the reduction peaks on the CuO/TiO_2 samples occur at temperatures lower than the reduction temperatures of neat CuO demonstrating interaction between the copper and the support to varying extents. Literature [33, 34, 36] ascribes the lower temperature reduction peaks to highly dispersed CuO while the higher temperature peaks depict the reduction of larger CuO particles, endorsing the idea of more than one type of copper deposit on the TiO_2. It is also apparent from Figure 5 the distribution of copper between the various sites differs for the two samples. The IE CuO/TiO_2 is dominated by the low temperature peak suggesting a greater presence of finely dispersed copper which contrasts with the WI CuO/TiO_2 where the larger copper oxide deposits are more pronounced. The higher portion of fine copper deposits on the IE CuO/TiO_2, (and by inference) on the IE Cu/TiO_2, compared with the WI Cu/TiO_2 may be a contributing factor to the differences in hydrogen generation rates between the two materials. Meng et al. reported CuO/CeO_2 prepared by a surfactant-modified method showed much higher thermal stability and catalytic activity for low temperature CO oxidation compared to the one prepared by a conventional precipitation method, due to the presence of more highly dispersed Cu species strongly interacting with CeO_2.[37] Other factors such as the overall higher support surface area may also contribute to the enhanced activity displayed by the IE Cu/TiO_2.

Copper is known to be prone to partial photodissolution when supported on TiO_2 and illuminated which in some instances can benefit the reaction.[38] To identify whether copper photodissolution occurred in this reaction system and the impact, if any, this may have had on activity and/or deactivation, 5 mL liquid samples were taken from the solution after each cycle, filtered and the filtrate analysed for copper ions using ICP. The results (Supplementary information, Table S1) indicated copper photodissolution occurred to different extents for the two materials. In the case of IE Cu/TiO_2 0.9 % (1.62 mg/L) of the copper was released into the solution after three cycle reaction while for WI Cu/TiO_2, approximately 1.5 % (2.67 mg/L) was released. It also appears that by the end of the first reaction cycle the copper photodissolution process had reached equilibrium. Future work is needed to confirm whether copper photodissolution plays a role in this system.

Conclusions

An ion exchange method was used as the basis for preparing Cu/TiO_2 for photocatalytic hydrogen generation. Copper cations were exchanged with sodium cations in hydrothermally synthesised sodium titanate to provide copper titanate. The copper titanate was then calcined and reduced to give IE Cu/TiO_2. Characterisation of the IE Cu/TiO_2 suggested copper was present on the TiO_2 as larger, predominantly metallic copper deposits in conjunction with finer, more highly dispersed copper deposits. Oxidised copper was also observed on the IE Cu/TiO_2 which may have derived from oxidation of the finer copper deposits and/or surface of the larger copper deposits. Photocatalytic hydrogen production by the IE Cu/TiO_2 was assessed and compared with copper-impregnated TiO_2 containing a similar copper loading (~19 wt%). The IE Cu/TiO_2 displayed a ~44 % greater hydrogen generation capacity over 5 hours than the WI Cu/TiO_2. This difference in activity was maintained over repeated reaction cycles. The elevated activity demonstrated by the IE Cu/TiO_2 is tentatively attributed to its greater quantity of fine, highly dispersed copper deposits on the TiO_2 surface. The ion exchange method potentially provides a new means of preparing metallised TiO_2 photocatalysts with a high metal dispersion.

Acknowledgements

The work was financially supported by the Australian Research Council (DP0986398). Dr X. L. Zhang greatly appreciates the University of New South Wales for providing a Vice-Chancellor's Research Fellowship and Fellowship term extension with funding support (PS26752) and Faculty Research Grant support (PS35135). The authors would also like to acknowledge the UNSW Mark Wainwright Analytical Centre, and thank Dr. Bill Gong for his assistance with XPS, Dr. Yu Wang for his support with XRD, and Dr. Katie Levick for her help with HRTEM and elemental mapping.

Notes and references

School of Chemical Engineering, UNSW Australia, Sydney, NSW 2052, Australia. E-mail: r.amal@unsw.edu.au; xiaolizhang.z@gmail.com; Fax: +61 293855966; Tel: +61 293854361.

‡Author contributions: X. L. Z. proposed the research and experimental design. H. T. carried out the materials synthesis, characterization, analysis and hydrogenation under a daily-based supervision from X. L. Z. and C. N., with further contributions from frequent discussions with J. S. and R. A.. H.T. performed the TPR analysis and interpreted the result with J. S..

†Electronic Supplementary Information (ESI) available: [TEM of sodium titanate, EDX compositional mapping analysis of ion-exchanged copper titanate, EDX compositional mapping analysis of IE Cu/TiO_2, XRD of pure TiO_2, WI CuO/TiO_2 and WI Cu/TiO_2, TEM images of WI Cu/TiO_2, core level XPS of Cu 2p from WI Cu/TiO_2 and ICP results of Cu^{2+} concentration leached from IE Cu/TiO_2 and WI Cu/TiO_2 into the aqueous solution in the three photocatalytic cycle measurements of hydrogen production]. See DOI: 10.1039/b000000x/

1. J. A. Turner, *Science*, 2004, **305**, 972-974.
2. R. M. Navarro, M. C. Sanchez-Sanchez, M. C. Alvarez-Galvan, F. del Valle and J. L. G. Fierro, *Energy Environ. Sci.*, 2009, **2**, 35-54.
3. M. Ni, M. K. H. Leung, D. Y. C. Leung and K. Sumathy, *Renew. Sust. Energy Rev.*, 2007, **11**, 401-425.
4. A. Cant, F. Huang, X. L. Zhang, Y. Chen, Y.-B. Cheng, R. Amal. *Nanoscale*, 2014, DOI: 10.1039/C3NR05456J.
5. J. C. Yu, J. G. Yu, W. K. Ho, Z. T. Jiang and L. Z. Zhang, *Chem. Mater.*, 2002, **14**, 3808-3816.
6. X. L. Zhang, Y. Chen, A. Cant, F. Huang, Y.-B. Cheng, R. Amal, *Part. Part. Syst. Charact.*, 2013, **30**, 754-758.
7. S. Kim and W. Choi, *J. Phys. Chem. B*, 2002, **106**, 13311-13317.
8. V. Subramanian, E. E. Wolf and P. V. Kamat, *J. Am. Chem. Soc.*, 2004, **126**, 4943-4950.
9. S. Sakthivel, M. V. Shankar, M. Palanichamy, B. Arabindoo, D. W. Bahnemann and V. Murugesan, *Water Res.*, 2004, **38**, 3001-3008.
10. B. A. Andersson, *Prog. Photovolt: Res. Appl.*, 2000, **8**, 61-76.
11. S. P. Xu and D. D. Sun, *Int. J. Hydrogen Energy*, 2009, **34**, 6096-6104.

12. J. Bandara, C. P. K. Udawatta and C. S. K. Rajapakse, *Photochem. Photobiol. Sci.*, 2005, **4**, 857-861.
13. N. L. Wu and M. S. Lee, *Int. J. Hydrogen Energy*, 2004, **29**, 1601-1605.
14. H. J. Choi and M. Kang, *Int. J. Hydrogen Energy*, 2007, **32**, 3841-3848.
15. Z. L. Jin, X. J. Zhang, Y. X. Li, S. B. Li and G. X. Lu, *Catal. Commun.*, 2007, **8**, 1267-1273.
16. K. Lalitha, G. Sadanandam, V. D. Kumari, M. Subrahmanyam, B. Sreedhar and N. Y. Hebalkar, *J. Phys. Chem. C.*, 2010, **114**, 22181-22189.
17. Y. Q. Wu, G. X. Lu and S. B. Li, *Catal. Lett.*, 2009, **133**, 97-105.
18. R. Takahashi, S. Sato, T. Sodesawa, M. Kato and S. Yoshida, *J. Sol-Gel Sci. Technol.*, 2000, **19**, 715-718.
19. T. Sodesawa, *React. Kinet. Catal. Lett.*, 1984, **24**, 259-264.
20. Z. T. Liu, D. S. Lu and Z. Y. Guo, *Appl. Catal. A-Gen.*, 1994, **118**, 163-171.
21. J. B. Rivest and P. K. Jain, *Chem. Soc. Rev.*, 2013, **42**, 89-96.
22. K. Kiatkittipong, J. Scott and R. Amal, *ACS Appl. Mater. Inter.*, 2011, **3**, 3988-3996.
23. N. Li, L. D. Zhang, Y. Z. Chen, M. Fang, J. X. Zhang and H. M. Wang, *Adv. Funct. Mater.*, 2012, **22**, 835-841.
24. X. M. Sun and Y. D. Li, *Chem. Eur. J.*, 2003, **9**, 2229-2238.
25. C. J. G. Vandergrift, A. F. H. Wielers, B. P. J. Joghi, J. Vanbeijnum, M. Deboer, M. Versluijshelder and J. W. Geus, *J. Catal.*, 1991, **131**, 178-189.
26. G. Diaz, R. Perez-Hernandez, A. Gomez-Cortes, M. Benaissa, R. Mariscal and J. L. G. Fierro, *J. Catal.*, 1999, **187**, 1-14.
27. G. A. Somorjai and G. Jernigan, *J. Catal.,* 1997, **165**, 284-284.
28. D. Tahir and S. Tougaard, *J. Phys.: Condens. Matter*, 2012, **24**, 175002.
29. J. J. Li, J. L. Zeng, L. S. Jia and W. P. Fang, *Int. J. Hydrogen Energy*, 2010, **35**, 12733-12740.
30. H. Praliaud, S. Mikhailenko, Z. Chajar and M. Primet, *Appl. Catal. B-Environ.*, 1998, **16**, 359-374.
31. K. Y. Song, Y. T. Kwon, G. J. Choi and W. I. Lee, *Bull. Korean Chem. Soc.*, 1999, **20**, 957-960.
32. J. G. Yu and J. R. Ran, *Energy Environ. Sci.*, 2011, **4**, 1364-1371.
33. Z. G. Liu, R. X. Zhou and X. M. Zheng, *Catal. Commun.*, 2008, **9**, 2183-2186.
34. Z. W. Huang, F. Cui, H. X. Kang, J. Chen, X. Z. Zhang and C. G. Xia, *Chem. Mater.*, 2008, **20**, 5090-5099.
35. S. Braun, L. G. Appel, V. L. Camorim and M. Schmal, *J. Phys. Chem. B*, 2000, **104**, 6584-6590.
36. X. L. Tang, B. C. Zhang, Y. Li, Y. D. Xu, Q. Xin and W. J. Shen, *Appl. Catal. A-Gen.*, 2005, **288**, 116-125.
37. Z. Q. Zou, M. Meng, L. H. Guo and Y. Q. Zha, *J. Hazard. Mater.*, 2009, **163**, 835-842.
38. S. W. Lam, M. Hermawan, H. M. Coleman, K. Fisher and R. Amal, *J Mol Catal A-Chem*, 2007, **278**, 152-159.